24th EUROPEAN ROTORCRAFT FORUM
Marseilles, France - 15th-17th September 1998

Rotary Wing Aeroelasticity in Forward Flight with Refined Wake Modelling

Référence : DY06

B. Buchtala and S. Wagner
Institut für Aerodynamik und Gasdynamik, Universität Stuttgart
Pfaffenwaldring 21, 70550 Stuttgart, Germany

Abstract

A modular approach for the numerical simulation of the aeroelastic behavior of a multi–bladed helicopter rotor in forward flight is presented. For this purpose the structural dynamic model STAN is now extended to deal with multiple blades in arbitrary motion and furthermore coupled with the three–dimensional finite volume Euler solver for unsteady, compressible flows, INROT.

For the accurate prediction of the three–dimensional flow field the rotor wake has to be described appropriately. In the present approach two different methods, a Chimera technique and a free wake model to provide the boundary conditions at the outer grid boundary, are used to capture the wake.

The solution of the surface coupled two–field problem is found by the use of a staggered time–marching procedure. A higher–order staggered algorithm is presented that takes full advantage of the underlying characteristics of the applied solution methods.

To validate the coupled approach a BO–105 model rotor in low–speed and in high–speed level flight is investigated. The experimental data is based on the European cooperative research project HELINOISE.

Nomenclature

$\bar{\bar{e}}$	specific total absolute energy
$\mathbf{e}, \mathbf{f}, \mathbf{g}$	flux vectors in ξ, η, ζ direction
$\mathbf{f}$	structure boundary conditions
$\mathbf{f}_\mathrm{l}$	aerodynamic force vector
$\mathbf{F}$	flow state
$\mathcal{F}$	right–hand side of blade dynamics
$\mathbf{k}$	coriolis and centrifugal force vector
$\mathbf{m}_\mathrm{l}$	aerodynamic moment vector
$\mathbf{s}$	flow boundary conditions
$\mathbf{S}$	structure state
t	time
$\bar{u}, \bar{v}, \bar{w}$	absolute velocities
V	cell volume
β	flapping angle
δ	degrees of freedom vector
ε	relative error sum
ζ	lagging angle
ϑ_b	blade torsion angle
ξ, η, ζ	body–fitted coordinates
ρ	density
τ	time
ϕ	conservative variables vector
ψ	azimuth angle

Introduction

A helicopter rotor in forward flight is a complex multi–disciplinary system. The three–dimensional flow field at the helicopter rotor is compressible and to a high degree unsteady. The advancing blade is subjected to a high Mach number environment at small angles of attack whereas the retreating blade has to deal with low dynamic pressures at high angles of attack in a viscous dominated flow regime. Another important fact is that the wake trailed by a rotor blade lifting surface does not conveniently waft away to the behind in a more or less continuous fashion, but eventually remains close enough to interact with succeeding blades. The dynamic behavior of the complete helicopter rotor is determined by the elastic properties of the various blades and to a smaller extend by the design of the rotor hub.

Early studies of rotary wing aeroelasticity

sought to identify the salient features of a particular problem using a theoretical representation as simple as possible. Simple models are ideal, if they work. They are efficient, user friendly and promote the understanding of the underlying physics. However, the answers that they provide were found to be not completely satisfactory and, over the years, particularly with the growing capability of the computer, theoretical models have been gradually refined and improved. It is now recognized that good aeroelastic modelling requires a comprehensive representation of rotor dynamics and aerodynamics as well as sound numerical and computational procedures.

Todays aerodynamic methods are ranging from blade–element theory over potential methods with a prescribed or fixed wake geometry and the transonic small disturbance method to Euler and Navier–Stokes methods. One the other hand, the dynamic behavior of the rotor blades can be calculated by multiple rigid–body systems over elastic beam elements and finite–element beam elements up to multiple three–dimensional finite–element structures.

Applied Solution Methods

Elastic Blade Analysis

The elastic analysis of the rotor blades is based on the dynamic model STAN using multiple rigid bodies connected with hinges. In this framework, the dynamic behavior of the blades is approximated only by their first natural modes and eigenfrequencies. The connecting hinges are provided with springs and dampers – their characteristics represent the elastic properties of the blade. The considered degrees of freedom are flapping, lagging, and blade torsion.

Using d'Alembert's principle, the governing equations of motion can be deduced from simple momentum balances at the hinges. A detailed derivation can be found in [3]. The resulting system of second–order ordinary differential equations reads

$$\ddot{\delta} = \mathcal{F}(\delta, \dot{\delta}, \mathrm{f_I}, \mathrm{m_I}) \,. \tag{1}$$

The vector δ contains the dependent variables for flapping β, lagging ζ, and blade torsion ϑ_b. The vectors $\mathrm{f_I}$ and $\mathrm{m_I}$ denote the aerodynamic forces and moments, respectively. Equation (1) is solved via an explicit fourth–order Runge–Kutta method.

The straightforward integration of Equation (1) does not produce a periodically converged solution before several hundred rotor revolutions are performed. The reader should keep in mind that each integration step of the structural solver implies at least one solution of the complete three–dimensional flow field – in fact the most time consuming part of the coupled solution process. Therefore, an essential task of rotary wing aeroelasticity is to minimize the number of integrations until a converged solution is achieved. Due to this the following mnemonic oriented convergence acceleration method is used. The vector of inital values of the kN'th ($k \in \mathbb{N}$) rotor revolution is composed of the weighted initial values from N previous rotor revolutions:

$$\delta^{kN}_{0,\mathrm{mod}} = \frac{1}{\sum_{n=1}^{N} n} \cdot \left(\sum_{n=1}^{N} n \cdot \delta_0^{(k-1)N+n} \right) . \tag{2}$$

The superscripts denote the rotor revolution. N is an arbitrary parameter to be chosen. Numerical experiments have shown that N is best set to $N = 3$. In this special case we obtain for the modified starting values

$$\delta^{3}_{0,\mathrm{mod}} = \frac{1}{6}\delta^1_0 + \frac{2}{6}\delta^2_0 + \frac{3}{6}\delta^3_0 \tag{3}$$

$$\delta^{6}_{0,\mathrm{mod}} = \frac{1}{6}\delta^4_0 + \frac{2}{6}\delta^5_0 + \frac{3}{6}\delta^6_0 \tag{4}$$

$$\vdots$$

The reader can easily verify that in the limiting case of a fully converged solution the starting values remain unchanged. In Figure 1 the relative error sum defined as

$$\varepsilon = \frac{1}{N_\mathrm{blade}} \sum_{n=1}^{N_\mathrm{blade}} \sum_{\psi=\Delta\psi}^{360^\circ} \left(\frac{\Delta\delta}{\delta} \right)^2 \tag{5}$$

is shown for the considered degrees of freedom. All degrees of freedom exhibit a very stable and

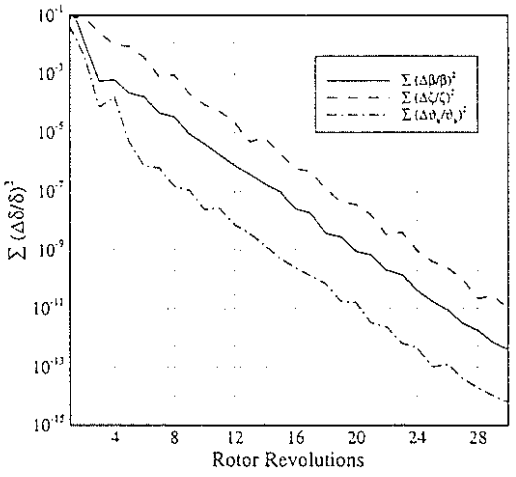

Figure 1: Transient Error Development

monotone convergence behavior. The convergence history of the blade torsion angle ϑ_b is depicted in Figure 2. It can be seen that the solution has converged to its periodic state at the end of the third revolution. Finally, two impor-

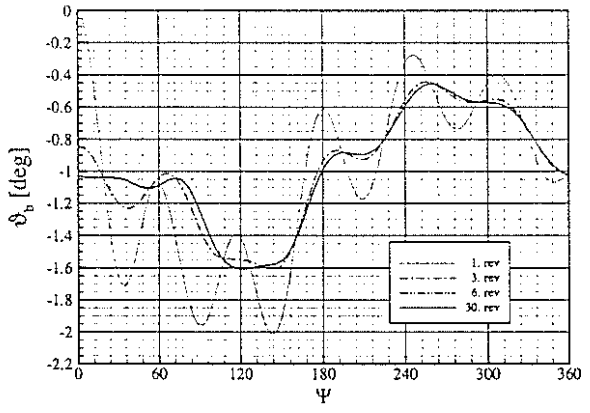

Figure 2: Convergence Study of Blade Torsion

tant properties of Equation (2) should be emphasized. First, due to the weighted assemblance of actual values out of previous ones, the solution development is damped in such a way that overshots will be prevented. This is not different to other underrelaxation schemes. The second and more important feature is that periodicity over a rotor revolution is enforced. Here we take advantage of the physical fact that for a fixed flight condition the solution has to be periodic.

Rotary Wing Aerodynamics

The three–dimensional, unsteady Euler equations are used to analyze the flow field around the helicopter rotor. They are formulated in a hub attached, non inertial rotating frame of reference with explicit contributions of centrifugal and coriolis forces.

The computational grid of a rotor blade is supposed to have an arbitrary motion relative to the rotating frame of reference. This is due to the cyclic pitch control as well as to the actual blade degrees of freedom. Thus, the Euler equations are formulated using time invariant body fitted coordinates [2, 23] :

$$\frac{\partial \phi}{\partial \tau} + \frac{\partial \mathrm{e}}{\partial \xi} + \frac{\partial \mathrm{f}}{\partial \eta} + \frac{\partial \mathrm{g}}{\partial \zeta} = \mathrm{k} \,. \qquad (6)$$

This so–called arbitrary Lagrangian–Eulerian (ALE) formulation allows each grid point to move with a distinct velocity in physical space, relative to the rotating reference system. The vector of the conservative variables, multiplied by the cell volume, is given by

$$\phi = V \cdot (\rho, \rho\bar{u}, \rho\bar{v}, \rho\bar{w}, \bar{\bar{e}}) \,. \qquad (7)$$

Here the velocity and energy are given in terms of absolute quantities. Krämer [12] showed that using absolute quantities obviates systematic numerical errors and therefore preserves uniform flow when using a rotating frame of reference. The flux vector components of e, f, and g as well as the force vector k can be found in [23, 27].

For the finite–volume cell centered scheme, the flow variables are assumed to be constant within the cell. Since their values undergo a variation throughout the flow field, discontinuities arise at the cell boundaries. The evaluation of the fluxes at the cell faces is done by an approximate Riemann solver developed by Eberle [6]. The uniformly high–order non oscillatory (UNO) scheme [11] is used for the spatial discretization.

Wake Modelling

The comprehensive simulation of multi–bladed rotors in forward flight has to take into account the reciprocal influence of the blades. The various blades affect themselves through their wakes, generated when lift is produced. Especially in flight situations with little downwash like low–speed level flight or descend flight the rotor blades strongly interact with their own wake system. In such cases the distinct vortices of the flow field have to be resolved and low–order models like global momentum theory are no longer applicable. In the present approach two different methods, both of them able to give an accurate prediction of the wake system, will be used to capture the wake.

Chimera Technique

One possible approach is to implicitly capture the wake of a helicopter rotor by the use of a sufficiently large computational domain which is able to resolve and transport the complete wake without further modeling. A separate grid is wrapped around each rotor blade. The individual blade grids are placed inside a base grid which covers the entire computational domain. The embedded grids exchange information at their boundaries with the base grid and hence with each other. Figure 3 shows the grid configuration of a four–bladed BO–105 helicopter rotor. The Chimera technique was incorporated

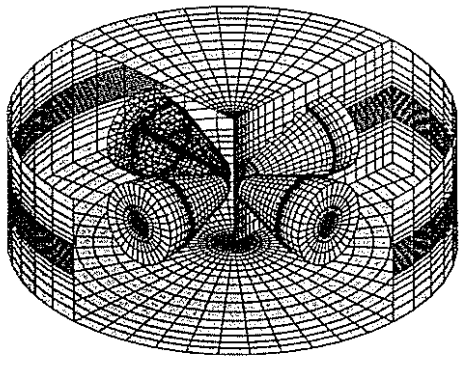

Figure 3: Chimera Grids

in the flow solver INROT by Stangl [23]. Due to the large number of gridpoints the computing time increases accordingly. Furthermore, additional time is needed for the search of transfer cells in the various grids. In order to minimize the required computing time, INROT was parallelized for shared memory architectures [27]. Each of the grids shown in Figure 3 is assigned to a processor. In order to achieve a good load balancing the base grid is divided into separate blocks, each with approximately the same number of grid points as the blade grids.

Free Wake Boundary Prescription

If the use of a computational domain enclosing all blades is not desired or possible, a free wake model can be used to provide the boundary conditions for a single blade grid in order to generate the wake which will subsequently be transported into the computational domain. Wehr showed in [26] that this procedure is indeed able to correcly capture the wake. The overall algorithm can be divided into three consecutive steps.

① First, the wake generated from the complete rotor over several revolutions is computed with the linear free wake vortex lattice method ROVLM by Zerle [28].

② Second, the solution from step ① is used to calculate the far field boundary conditions for the Euler calculation over a complete rotor revolution. Therefore it is necessary to position the computational grid of the Euler solver according to a prescribed motion of the rotor blade.

③ Third, the Euler solver INROT in conjunction with the dynamic module STAN computes the compressible, non linear flow field around the investigated blade as well its transient aeroelastic response.

Using the aforementioned procedure a realistic, three–dimensional flow field of a multi–bladed helicopter rotor can be computed. Figure 4 shows the vortex lattice after $2\,^1/_4$ rotor revolutions in low–speed forward flight. At $\psi = 90°$, a portion of the outer boundary of the Euler grid is shown, providing a view at the vortices of the

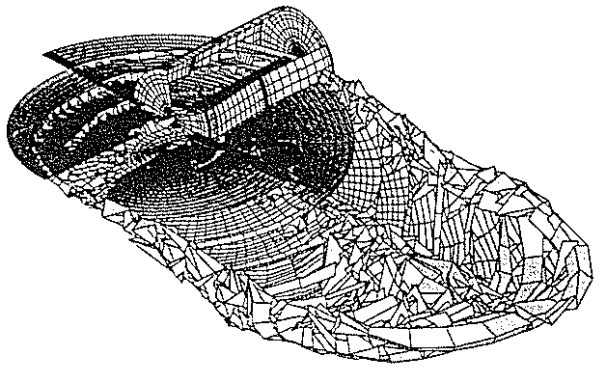

Figure 4: Wake Structure and Euler Grid

free wake inside the computational domain. The boundary conditions enforce the emergence and convection of these vortices in the course of solution phase ③.

The only drawback of this algorithm, when used in the framework of a fluid structure coupling process, is that the movement of the blade has to be prescribed in step ① as well as in step ②. During phase ③ the motion of the blade is likely to change. Now the already determined boundary conditions do no longer exactly represent the actual physical scenario. Increasing discrepancies between the actual and the initially presumed rotor position will cause growing inaccuracies in the overall outcome of the calculation. To circumvent this problem step ①–③ has to be repeated in an iterative manner until convergence is achieved.

Fluid Structure Coupling

During one rotor revolution the blades of the helicopter rotor are exposed to fast varying airloads. They affect the movement and deformation of the blade. In turn, the actual shape and velocity of the blade surface determines large parts of the flow field. We can state that the physical interaction between the fluid and the structure is restricted to the wetted surface of the blade. The time dependent state of the flow defines the boundary conditions of the structure through the surface forces, whereas the actual state of the structure determines the boundary conditions of the fluid flow through its shape and velocity.

In very simple and small-scale structural problems the coupled system can be solved in a way that combines the fluid and structural equations of motion into one single formulation. This monolithic set of differential equations describes the fully coupled fluid structure system as a unity. However, we have to deal with the nonlinear Euler equations. The governing equations for the structure may be linear or non linear. It has been pointed out in [14] that the simultaneous solution of these equations by a monolithic scheme is in general computationally challenging, mathematically suboptimal and from the point of software development unmanageable.

Alternatively, the fluid structure coupling can be accomplished by partitioned procedures [4]–[10], [13]–[21], [24], [25]. The fluid and structure partitions are processed by different programs with interactions only due to the external input of boundary conditions, provided at synchronisation points. In the meantime the fluid and the structure evolves independently, each one of them using the most appropriate solution technique. This approach offers several appealing features, including the ability to use well-established solution methods within each discipline, simplification of software development efforts, and preservation of software modularity.

The exchange of boundary conditions – surface forces to the structural code and blade motion to the fluid solver – is best done consistent with the integration scheme used. Therefore, integrating from time level t^n to t^{n+1}, the implicit flow solver INROT is provided with boundary conditions from time level t^{n+1}, whereas the explicit dynamic solver STAN obtains exchange data from time level t^n. Piperno proved in [18] that the inconsistent treatment of boundary conditions reduces the accuracy of the coupled system and eventually deteriorates the stability limit.

Staggered Algorithms

In [7, 18] various staggered algorithms for the explicit flow/implicit structure treatment of boundary conditions are presented. Staggered schemes of this type, as well as algorithms for explicit/explicit or implicit flow/explicit structure, permit the integration of the coupled system by solely two consecutive integration steps, one for each solver part. In [4] an adaption of the basic staggered scheme presented in [7, 18] to implicit flow/explicit structure solvers was presented. This scheme, denoted FSC1, is repeated in Figure 5 for convenience. In the depicted scheme, the superscripts correspond to the timelevel. $\mathbf{S}$, $\mathbf{s}$, $\mathbf{F}$, and $\mathbf{f}$ represent the state of the structure, the boundary conditions for the fluid flow, the state of the fluid, and the forces on the structure surface, respectively. The filled arrows $\longrightarrow$ represent heavy computations with high computational costs, i.e. updating the state of the fluid with known boundary conditions. The hollow arrows $\longrightarrow\!\triangleright$ represent computations with moderate or low computational costs, i.e. advancing the structure state, computing the boundary conditions for the flow, or calculating the surface force from the known variables of the fluid flow. The dashed lines indicate that additional information is needed. For example to determine the state of the structure $\mathbf{S}^{n+1}$ not only the forces $\mathbf{f}^n$ have to be known but also the previous state of the structure $\mathbf{S}^n$. The elementary steps are as follows.

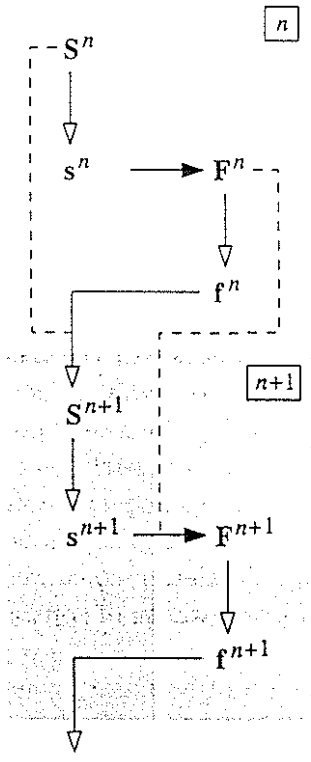

Figure 5: Fluid Structure Coupling Scheme 1

① Advance the structural system to $\mathbf{S}^{n+1}$ under a fluid induced load $\mathbf{f}^n$.

② Transfer the motion of the blade surface $\mathbf{s}^{n+1}$ to the fluid system.

③ Advance the fluid system to $\mathbf{F}^{n+1}$.

④ Compute the forces on the structure $\mathbf{f}^{n+1}$.

Such a partioned procedure can be described as a loosely coupled solution algorithm. Piperno proved in [18] that even when the underlying flow and structural solvers are second–order accurate in time, coupling schemes of the FSC1 type are only first–order accurate. For this reason other authors [16, 19, 24, 25] advocate iterating on steps ①–④ until the governing equations of motion are satisfied. Then the coupled system is advanced to the next time step. In the field of helicopter aerodynamics multiple iterations of the flow solver are beyond the boundaries of the overall computing time. Therefore, a higher–order predictor–corrector staggered scheme was developed that takes full advantage of the underlying characteristics of the employed solvers and the physics of the flow. Since the computing time of the dynamic code is negligible compared to the time needed for the flow field computation, the predictor–corrector procedure is restricted to the structure step only. The overall computing time remains almost unaffected. The algorithm additionally takes care of the physical fact that the typical time of evolution for the fluid is considerably smaller than for the structure. Rapid changes of the flow are easily captured by the coupled scheme since the predicted structure state is corrected at the end of the time step. The FSC2 algorithm depicted in Figure 6 consists of the following six steps.

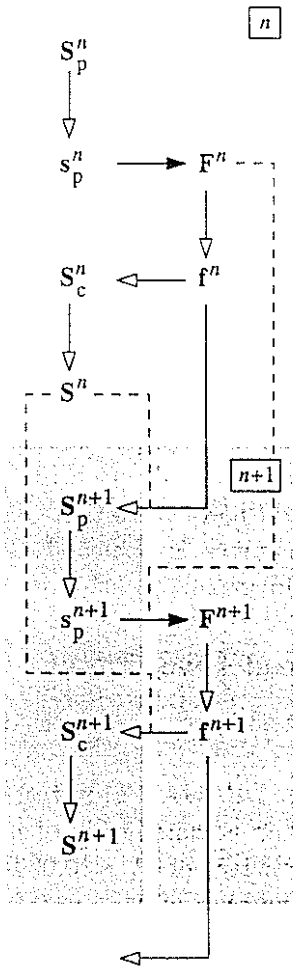

Figure 6: Fluid Structure Coupling Scheme 2

① Predict the structural state S_p^{n+1} under a fluid induced load f^n.

② Transfer the predicted motion of the blade surface s_p^{n+1} to the fluid system.

③ Advance the fluid system to F^{n+1}.

④ Compute the forces f^{n+1} on the structure.

⑤ Advance the structure one more time to the corrector state S_c^{n+1}, now under the fluid induced load f^{n+1}.

⑥ Take the average of predicted and corrected values as the final structure state

$$S^{n+1} = \frac{1}{2} \cdot \left(S_c^{n+1} + S_p^{n+1} \right). \qquad (8)$$

Figure 7 shows the torsional moment acting on a rotorblade, computed with coupling scheme FSC1 as well as FSC2 using different integration step sizes $\Delta\psi = 1^o, 5^o$ and 10^o. Using the

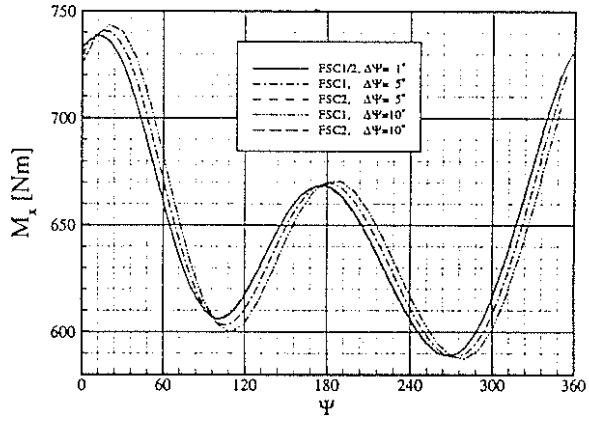

Figure 7: Comparison of Coupling Schemes

smallest step size of $\Delta\psi = 1^o$ the results obtained with FSC1 and FSC2 show no difference. The situation changes when larger step sizes are used. Coupling scheme FSC2 still gives the same results even when the step size is increased to $\Delta\psi = 10^o$. This is not the case when scheme FSC1 is used for coupling. Then a systematic numerical error become evident. The amplitude as well as the phase of the curve change at larger stepsizes.

In order to retain the advantage of software modularity, given by the use of partitioned procedures, the fluid and the structure code are kept as separate programs. They communicate with each other by means of message queues. Message queues are part of the UNIX–System VR4 interprocess communication routines. When the computation gets started, two message queues are set up. One queue is used to provide the structural code with aerodynamic loads, the other one to transfer the blade coordinates and velocities to the fluid solver. Each message that will be put on the message queue stack is provided with an identifier for the blade the transmitted data belongs to. Further details of the implementation can be found in [5].

Results and Discussion

The validation of the coupled codes is done on a BO–105 model rotor. The test campaign at the DNW, carried out within the framework of the European cooperative research project HELINOISE, provides an extensive database for different flight conditions simulated with a 40% geometrically and dynamically scaled model of the BO–105 helicopter [22].

The rotor under consideration is a four–bladed hingeless rotor with a diameter of 4 m, a root cut–out of 0.350 m, and a chord length of 0.121 m. The rotor blade uses a NACA 23012 airfoil with the trailing edge modified to form a 5 mm long tab to match the geometry of the full–scale rotor. The rotor blades have -8^o of linear twist, a standard square tip, and a solidity of 0.077. The nominal rotor operational speed is 1040 rpm.

The elastic rotor blade is represented with three degrees of freedom accounting for flapping, lagging and blade torsion.

The Chimera technique uses four blade grids and a base grid for the discretization of the entire flow field. These grids have already been shown in Figure 3. The number of grid points are summarized in the following table.

Blade Grid	Base Grid	Total
$65 \cdot 47 \cdot 18$	$85 \cdot 51 \cdot 49$	$4 \cdot 54990 + 212415$
$= 54990$	$= 212415$	$= 432375$

The calculation is done on a NEC–SX4 supercomputer. When working in parallel with eight processors and with a performance of approximately 600 MFlops per processor one rotor revolution takes about 2h 30min. The number of revolutions that have to be performed in order to get a converged solution of the coupled system depends on the flight conditions. Roughly speaking between two and four revolutions are sufficient in almost any case.

When the free wake boundary prescription technique is employed a finer blade grid with a total number of $129 \cdot 83 \cdot 31 = 331917$ grid points is used. Furthermore, compared to the Chimera blade grids, the distance of the outer boundary from the blade is reduced from ten chord lengths down to five. This is done in order to get a better resolution of the incoming wake. The computing time needed for the separate steps of the algorithm outlined in the section *Free Wake Boundary Prescription* is shown in the following table.

Free Wake	Boundary Conditions	Coupled Euler Calculation
1h	3h	2h

The given values form the basis for the first rotor revolution. Further rotor revolutions contribute to the total time only with the time needed for the coupled Euler calculation. As in the Chimera case convergence is achieved after two to four rotor revolutions.

Low–Speed Level Flight

The first test–case chosen for the validation of numerical results is the low–speed level flight, HELINOISE DP–344. This test–case is characterized by an advance ratio of $\mu = 0.15$, a rotor thrust coefficient of $C_t = 0.00446$, and a hover tip Mach number of $\mathrm{Ma_h} = 0.644$. Further details can be found in [22].

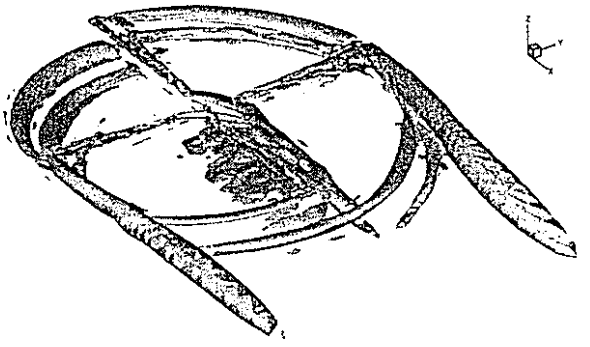

Figure 8: Wake System DP–344

Figure 8 shows the system of wake vortices encountered. It becomes clear that the coupled algorithm has to deal with various blade vortex interactions at different azimuthal and radial locations.

The Figures 9–11 show the resulting blade degrees of freedom β, ζ and ϑ_b. The solid lines denote the results obtained with the Chimera technique whereas the dashed lines denote the calculations done with free wake boundary conditions. Except for the flapping angle β both results agree fairly well. The flapping angle seems to be quite sensitive to the aerodynamic modelling of the wake. It is probable that better correspondance is achieved if the free wake boundary conditions are re–calculated in a second cycle using the actual degrees of freedom.

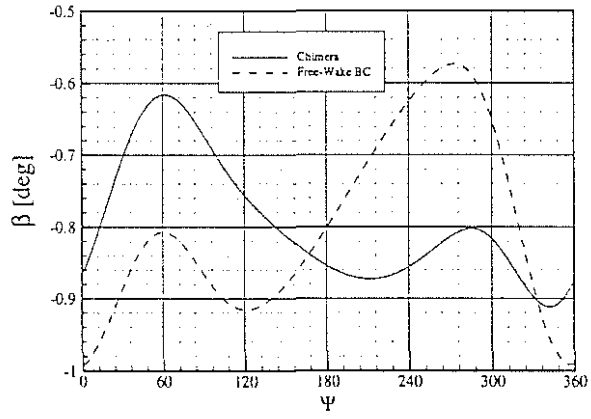

Figure 9: Flapping Angle DP–344

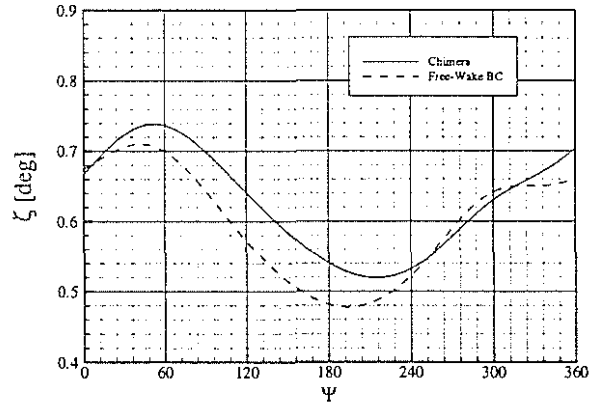

Figure 10: Lagging Angle DP–344

The spanwise forces and moments shown in Figure 16 over a rotor revolution are obtained when the pressure is integrated over the blade section. This is done at the radial blade sections

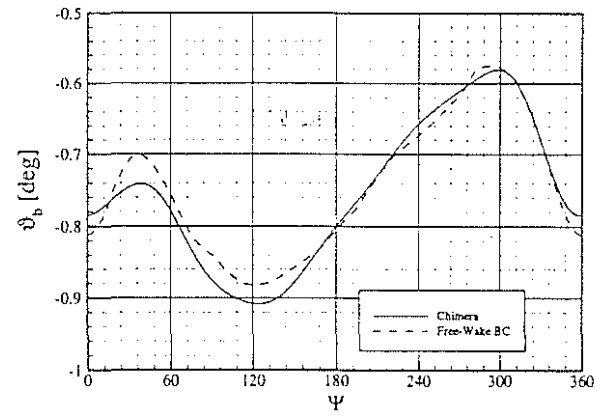

Figure 11: Blade Torsion Angle DP–344

$r/R = 0.75$ and $r/R = 0.79$ The x–axis of the underlying coordinate system points towards the trailing edge of the blade section, the y–axis to the blade tip, and the z–axis upwards. A comparison is made between the Experiment, the Chimera technique, the free wake boundary prescription model, and a calculation done without blade dynamics. The uncoupled rigid blade calculation overpredicts the experimental forces and moments in almost any case. This is no surprise since the blade undergoes torsion in the coupled calculation as can be seen in Figure 11. Since the angle of attack is directly coupled to any variation of ϑ_b it becomes clear that neglecting blade torsion might lead to insufficient results. In comparison to ϑ_b, the direct impact of β and ζ on the aerodynamic forces and moments is rather small. They affect the aerodynamic loads primarily through their time derivates, which are quite small if we take a look at Figure 9 and 10. At $r/R = 0.97$ the force and moment distributions show that blade vortex interactions have taken place at $\psi = 80^o$ and $\psi = 280^o$. The results of the free wake boundary prescription model evidently give a better resolution of the vortices but sometimes lead to an overprediction of vortex strength at $\psi = 60^o$. As mentioned earlier this symptom could possibly be corrected with an re–calculation of boundary conditions using the actual degrees of freedom. In general the calculated forces and moments are in good agreement with the experimental data ex-

cept for dM_y/dr at $r/R = 0.97$. In this case the calculated torsional moment is considerably smaller than the measured one. Since dM_y/dr at $r/R = 0.75$ is in a significantly better agreement with the experiment one possible cause for this behavior is that in our calculation model we used a constant torsional angle over the blade – this is not the case for the real blade where the torsion angle varies over the blade axis. This fact might also be one possible reason for the significant drop in dF_z/dr and dM_z/dr at $\psi = 150^o$ which cannot be reproduced by the calculation.

Comparisons between the experimental chordwise pressure distributions and calculated results are presented in Figure 17 for various azimuthal and radial positions. Very good agreement between calculated and measured distributions is observed. The deviation at $\psi = 360^o$, $r/R = 0.75$ is due to the undisturbed inboard wake, which is not present in the experiment due to the rotor hub.

High–Speed level flight

The second test case, used for the validation of the coupled approach is a helicopter rotor in high–speed level flight, HELINOISE DP–1839. This test case is characterized by an advanced ratio of $\mu = 0.337$, a rotor thrust coefficient of $C_t = 0.00458$, and a hover tip Mach number of $\mathrm{Ma_h} = 0.674$.

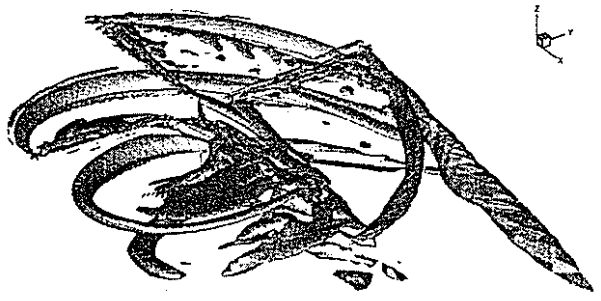

Figure 12: Wake System DP–1839

The wake system is visualized in Figure 12. Unlike the previous case the rotor is not subjected to blade vortex interactions due to the increased downwash since the rotor shaft is tilted forward at an angle of 9.8°. We now have the situation that shocks occur at the advancing blade.

The degrees of freedom flapping, lagging and blade torsion are shown in the Figures 13–15 over one rotor revolution. The results obtained with the Chimera method agree very well with those calculated with the free wake boundary conditions. Regarding the blade torsion angle short wave oscillations are damped when the Chimera method is used. This is likely due to the coarser and therefore more dissipative grid used in the Chimera calculations.

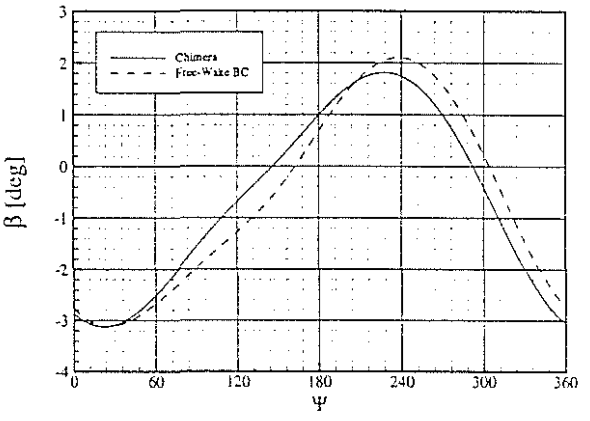

Figure 13: Flapping Angle DP–1839

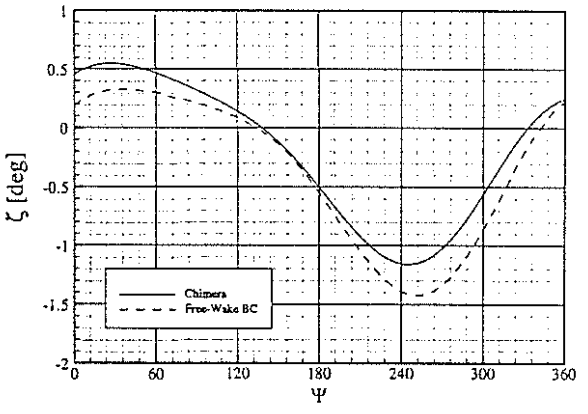

Figure 14: Lagging Angle DP–1839

The forces and moments per units span

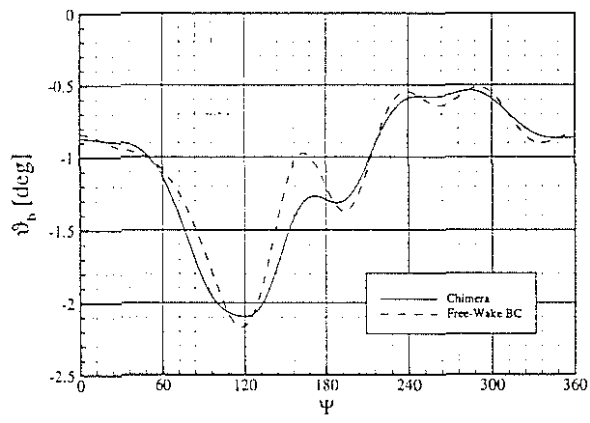

Figure 15: Blade Torsion Angle DP–1839

dF_x/dr, dF_z/dr, dM_y/dr, and dM_z/dr are shown in Figure 18. A purely aerodynamic calculation, indicated by the dotted lines, is in no way capable of predicting the experimentally determined values. The situation changes if the dynamic properties of the blade are taken into account. The coupled results show the same characteristical course as the experimental data. However, between $\psi = 0^o$ and $\psi = 180^o$ we still have a discrepancy in amplitude and phase, especially at $r/R = 0.79$. The differences between the calculated results and measured data need further investigations. It has to be scrutinized if the deviations belong to the simple dynamic model used in the coupled approach which cannot account for the fully elastic properties of the real blade.

Figure 19 shows the chordwise pressure distributions calculated with the Chimera method as well as the measured ones. In this picture the same solution properties as in Figure 18 become visible. The coupled scheme is able to capture the qualitative characteristics of the experimental pressure distributions in an acceptable way.

Conclusions and Outlook

In this paper we presented an approach for the aeroelastic analysis of multi–bladed helicopter rotors in forward flight. The dynamic properties of the various blades are represented by a rather simple model that takes only the first natural modes and eigenfrequencies into account. The flow field is described by the three dimensional Euler equations, numerically solved with a cell centered finite volume upwind scheme.

Two different methods for an accurate prediction of the rotor wake were used. On one hand a Chimera technique where the wake is captured by the use of a sufficiently large computational domain was applied. On the other hand a free wake model was used to provide realistic wake boundary conditions for a single blade grid. Both approaches seemed to give almost equal results concerning the predicted flow field as well as the resulting dynamic behavior of the blade obtained during the coupling process.

A higher–order staggered procedure was presented and compared with a first–order scheme. The higher–order scheme allows about ten times larger time steps without loosing accuracy. Moreover, the overall computing time remains almost unaffected by the higher–order scheme since it take full advantage of the underlying characteristics of the applied solution methods.

The validation of the aeroelastic system is done on a BO–105 model rotor in low–speed and high–speed level flight. The results show that neglecting the dynamic properties of the blade lead to unsatisfactory results. The coupled results of the low–speed level flight are in good agreement with the experimental data. The flapping angle turned out to be very sensitive to the spatial position and strength of the incoming vortices. The simple dynamic model currently used is not capable to achieve such a good agreement of calculated and measured data as in the low–speed flight case. However, the coupled results are in much better agreement with the experiment than the results achieved with a purely aerodynamic calculation. It is likely that the above mentioned shortcomings belong to the simple dynamic model used in the calculation procedure.

Current work deals with the incorporation of the developed methods in helicopter trim calculation procedures. Future work will be done on the development and application of higher–order coupling schemes with a higher degree of modularity. Furthermore a refined dynamic model of a fully elastic blade has to be taken into consideration.

Acknowledgement

This work was supported by the BMBF under the reference number 20H–9501–B. The author would like to thank Eurocopter Deutschland for providing him with the structural data for the dynamic calculations.

References

[1] Batina, J.T.: *Unsteady Euler Airfoil Solutions using Unstructured Dynamic Meshes.* AIAA paper 89–0115, 27th AIAA Aerospace Sciences Meeting, Reno, Nevada, January 1989.

[2] Brenneis, A.: *Berechnung instationärer zwei– und dreidimensionaler Strömungen um Tragflügel mittels eines impliziten Relaxationsverfahrens zur Lösung der Eulergleichungen.* Ph.D. Thesis, Institut für Luftfahrttechnik und Leichtbau, Universität der Bundeswehr München, Neubiberg, 1989.

[3] Buchtala, B.: *STAN Programmbeschreibung. Theoretische Grundlagen zur Berechnung des Hauptrotors.* Internal Report, Institut für Aero– und Gasdynamik, Universität Stuttgart, Germany, August 1996.

[4] Buchtala, B., Wehr, D., and Wagner, S.: *Coupling of Aerodynamic and Dynamic Methods for the Calculation of Helicopter Rotors in Forward Flight.* 23rd European Rotorcraft Forum, pp. 5.1–5.12, Dresden, September 1997.

[5] Buchtala, B., Wagner, S.: *Gekoppelte Berechnung der Dynamik und Aerodynamik von Drehflüglern.* 3. Zwischenbericht, Förderkennzeichen 20H 9501 B, Institut für Aero– und Gasdynamik, Universität Stuttgart, April 1998.

[6] Eberle, A.: *MBB–EUFLEX. A New Flux Extrapolation Scheme Solving the Euler Equations for Arbitrary 3–D Geometry and Speed.* Report MBB–LKE122–S–PUB–140, MBB, Ottobrunn, Germany, 1984.

[7] Farhat, C., Lesoinne, M., Chen, P.S., and Lantéri, S.: *Parallel Heterogeneous Algorithms for the Solution of Three–Dimensional Transient Coupled Aeroelastic Problems.* AIAA paper 95–1290, 36th AIAA Structures, Structural Dynamics and Materials Conference, New Orleans, Louisiana, April 1995.

[8] Felippa, C.A. and Geers, T.L.: *Partitioned Analysis for Coupled Mechanical Systems.* Engineering Computations, vol. 5, pp. 123–133, June 1988.

[9] Gupta, K.K.: *Development of a Finite Element Aeroelastic Analysis Capability.* Journal of Aircraft, vol. 33, pp. 995–1002, 1996.

[10] Guruswamy, G.P.: *Time–Accurate Unsteady Aerodynamic and Aerolelastic Calculations of Wings using Euler Equations.* AIAA paper 88–2281, 29th AIAA Structures, Structural Dynamics and Materials Conference, Williamsburg, Virginia, April 1988.

[11] Harten, J. and Osher, S.: *Uniformly High–Order Nonoscillatory Schemes I.* SIAM Journal on Numerical Analysis, vol. 24, pp. 279–309, 1987.

[12] Krämer, E.: *Theoretische Untersuchungen der stationären Rotorblattumströmung mit Hilfe eines Euler–Verfahrens.* Ph.D. Thesis, Institut für Luftfahrttechnik und Leichtbau, Universität der Bundeswehr München, Neubiberg, 1991.

[13] Lee–Rausch, E.M. and Batina, J.T.: *Wing–Flutter Boundary Prediction using Unsteady Euler Aerodynamic Method.* AIAA paper 93–1422, 34th AIAA Structures, Structural Dynamics and Materials Conference, La Jolla, California, April 1993.

[14] Lesoinne, M. and Farhat, C.: *Improved Staggered Algorithms for the Serial and Parallel Solution of Three–Dimensional Nonlinear Transient Aeroelastic Problems.* Fourth World Conference on Computational Mechanics, E. Onate and S.R. Idelsohn, editors, Barcelona, Spain, 1998.

[15] Morton, S.A. and Beran, P.S.: *Nonlinear Analysis of Airfoil Flutter at Transonic Speeds.* AIAA paper 95–1905, 13th AIAA Applied Aerodynamics Conference, San Diego, June 1995.

[16] Mouro, J.: *Numerical Simulation of Nonlinear Fluid Structure Interactions Problems and Application to Hydraulic Shock–Absorbers.* Third World Conference in Applied Computational Fluid Dynamics, Basel, May 1996.

[17] Park, K.C. and Felippa, C.A.: *Computational Methods for Transient Analysis.* In T. Belytschko and T.J.R. Hughes, editors, *Partitioned analysis of coupled systems*, pp. 157–219, North–Holland Pub. Co., 1983.

[18] Piperno, S., Farhat, C., and Larrouturou, B.: *Partitioned Procedures for the Transient Solution of Coupled Aeroelastic Problems, Part I: Model Problem, Theory and Two-Dimensional Application.* Computer Methods in Applied Mechanics and Engineering, vol. 124, no. 1–2, pp. 79–112, June 1995.

[19] Pramono, E. and Weeratunga, S.K.: *Aeroelastic Computations for Wings through Direct Coupling on Distributed-Memory MIMD Parallel Computers.* AIAA paper 94–0095, 32nd AIAA Aerospace Sciences Meeting, Reno, Nevada, January 1994.

[20] Rausch, R.D., Batina, J.T., and Yang, T.Y.: *Euler Flutter Analysis of Airfoils using Unstructured Dynamic Meshes.* AIAA paper 89–13834, 30th AIAA Structures, Structural Dynamics and Materials Conference, Mobile, Alabama, April 1989.

[21] Smith, J.M.: *Flight Loads Prediction Methods for Aircraft: Vol. I, Euler/Navier–Stokes Aeroelastic Method (ENS3DAE), Technical Development Summary: Version 4.0.* WRDC–TR–89–3104, November 1989.

[22] Splettstoesser, W.R., Junker, B., Schultz, K.–J., Wagner, W., Weitemeyer, W., Protopsaltis, A., and Fertis, D.: *The HELINOISE Aeroacoustic Rotor Test in the DNW - Test Documentation and Representative Results.* DLR–Mitteilung 93–09, Braunschweig, December 1993.

[23] Stangl, R.: *Ein Eulerverfahren zur Berechnung der Strömung um einen Hubschrauber im Vorwärtsflug.* Ph.D. Thesis, Institut für Aero– und Gasdynamik, Universität Stuttgart, 1996.

[24] Strganac, T.W. and Mook, D.T.: *Numerical Model of Unsteady Subsonic Aeroelastic Behavior.* AIAA Journal, vol. 28, pp. 903–909, 1990.

[25] Weeratunga, S.K. and Pramono, E.: *Direct Coupled Aeroelastic Analysis through Concurrent Implicit Time Integration on a Parallel Computer.* AIAA paper 94–1550, 35th AIAA Structures, Structural Dynamics and Materials Conference, Hilton Head, South Carolina, April 1994.

[26] Wehr, D., Zerle, L., and Wagner, S.: *Coupling Euler and Potential Methods for the Calculation of Rotors in Unsteady Forward Flight.* 22nd European Rotorcraft Forum, pp. 59.1–59.12, Brighton, September 1996.

[27] Wehr, D.: *Untersuchungen zum Wirbeltransport bei der Simulation der instationären Umströmung von Mehrblattrotoren mittels der Eulergleichungen.* Ph.D. Thesis, Institut für Aero– und Gasdynamik, Universität Stuttgart, 1998.

[28] Zerle, L.: *Aerodynamische und aeroakustische Rotorberechnung unter Anwendung retardierender Potentiale* Ph.D. Thesis, Institut für Aero– und Gasdynamik, Universität Stuttgart, 1998.

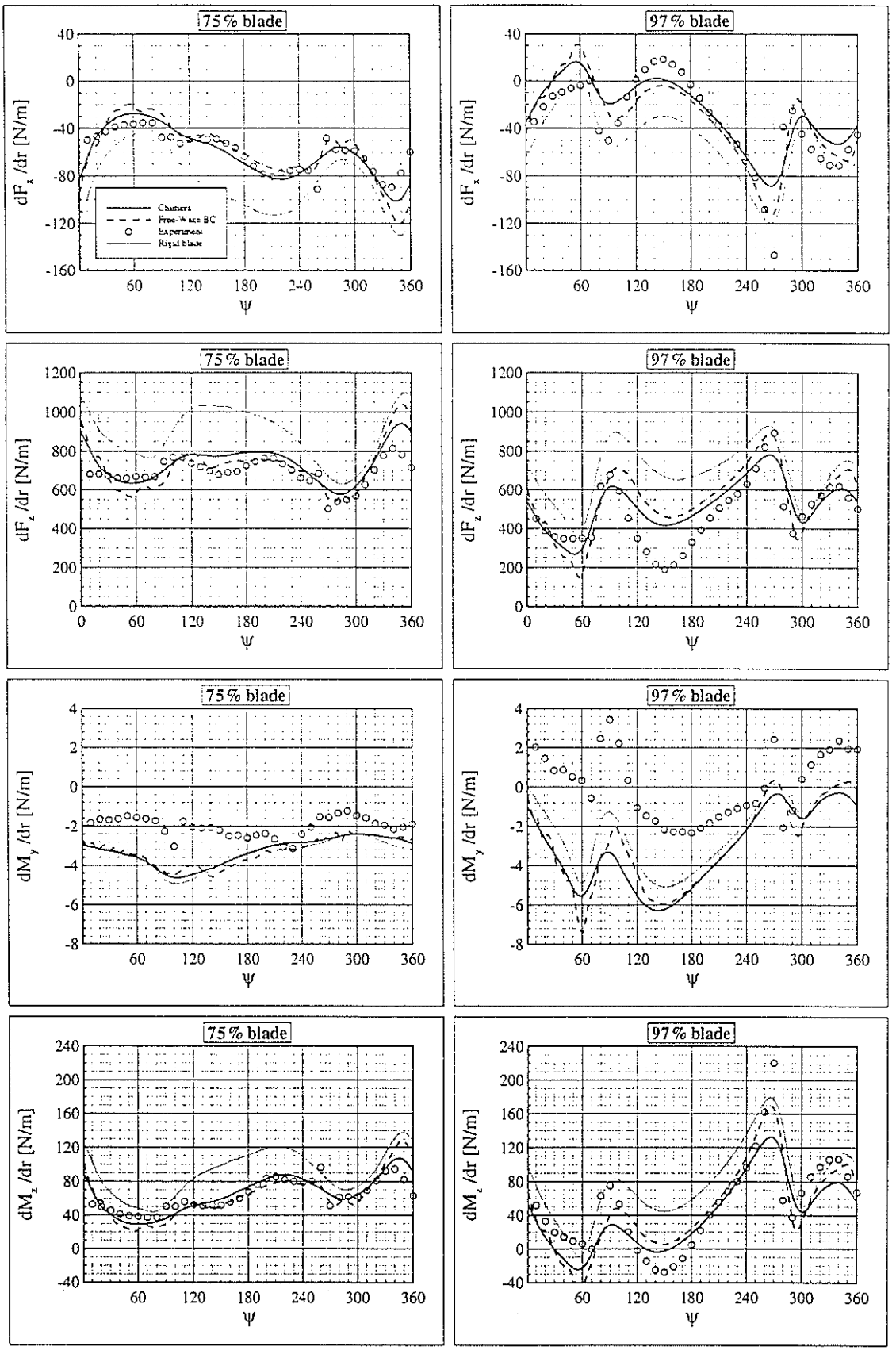

Figure 16: Forces and Moments DP–344

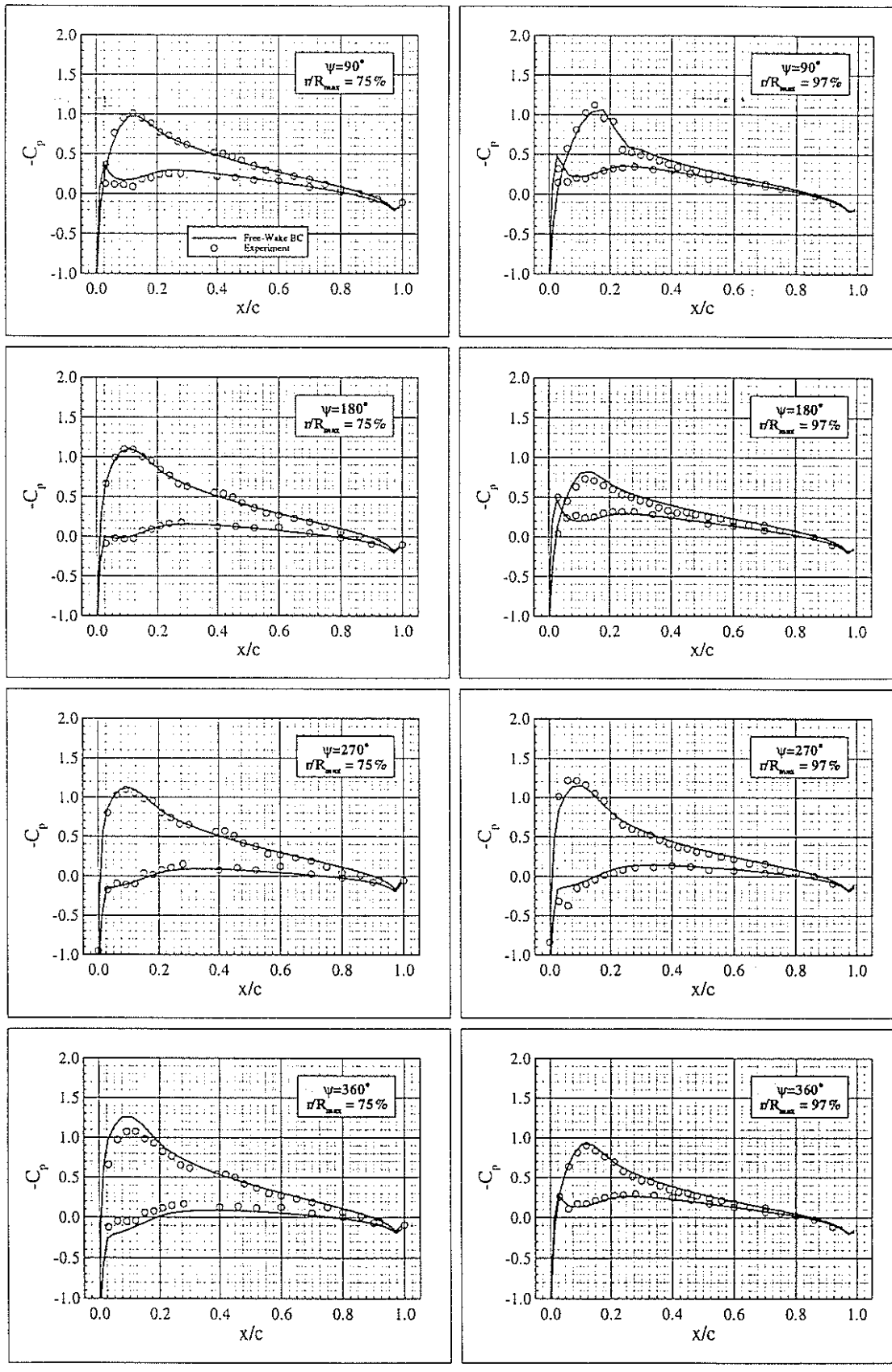

Figure 17: Chordwise Pressure Distributions DP–344

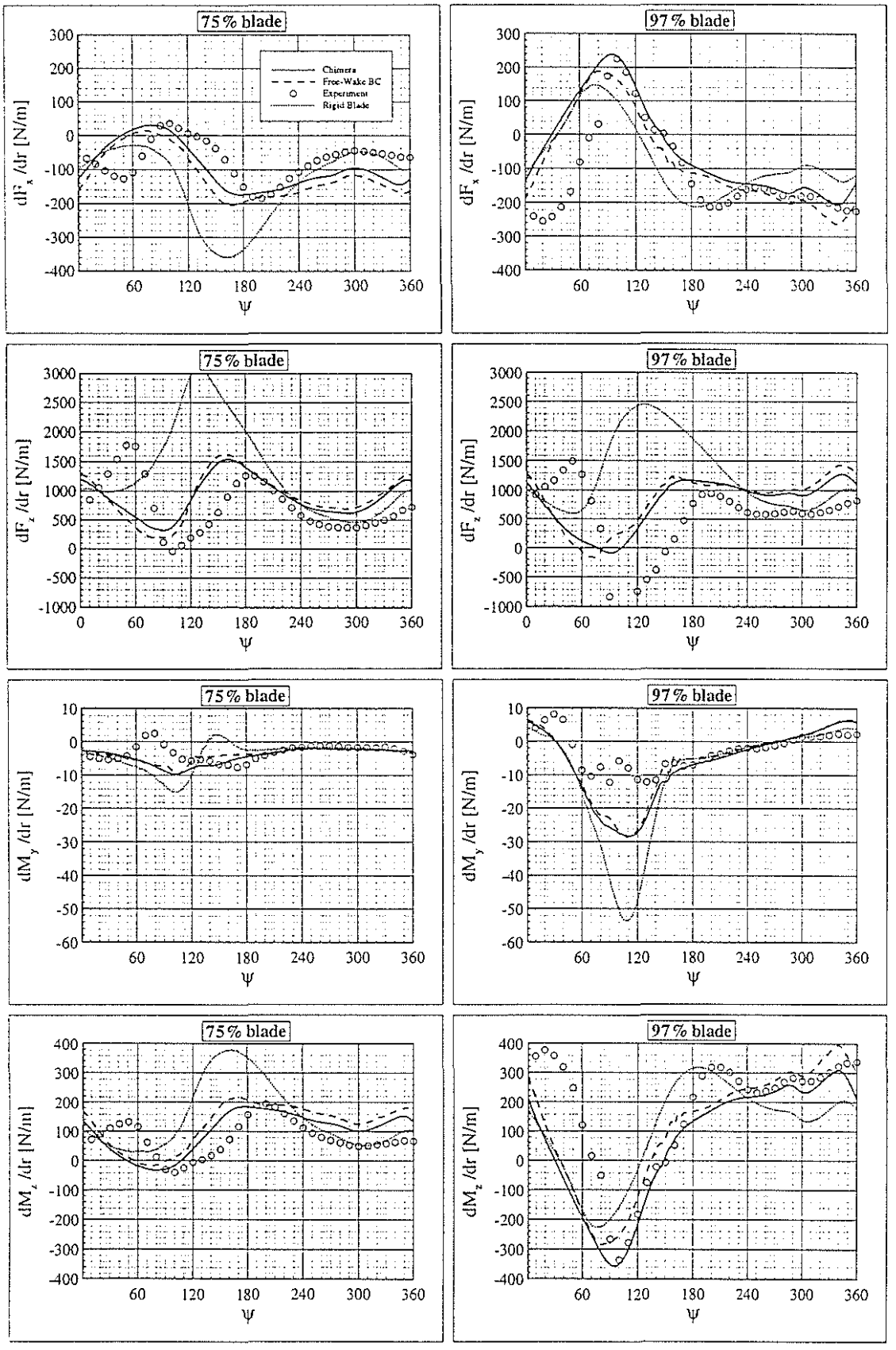

Figure 18: Forces and Moments DP--1839

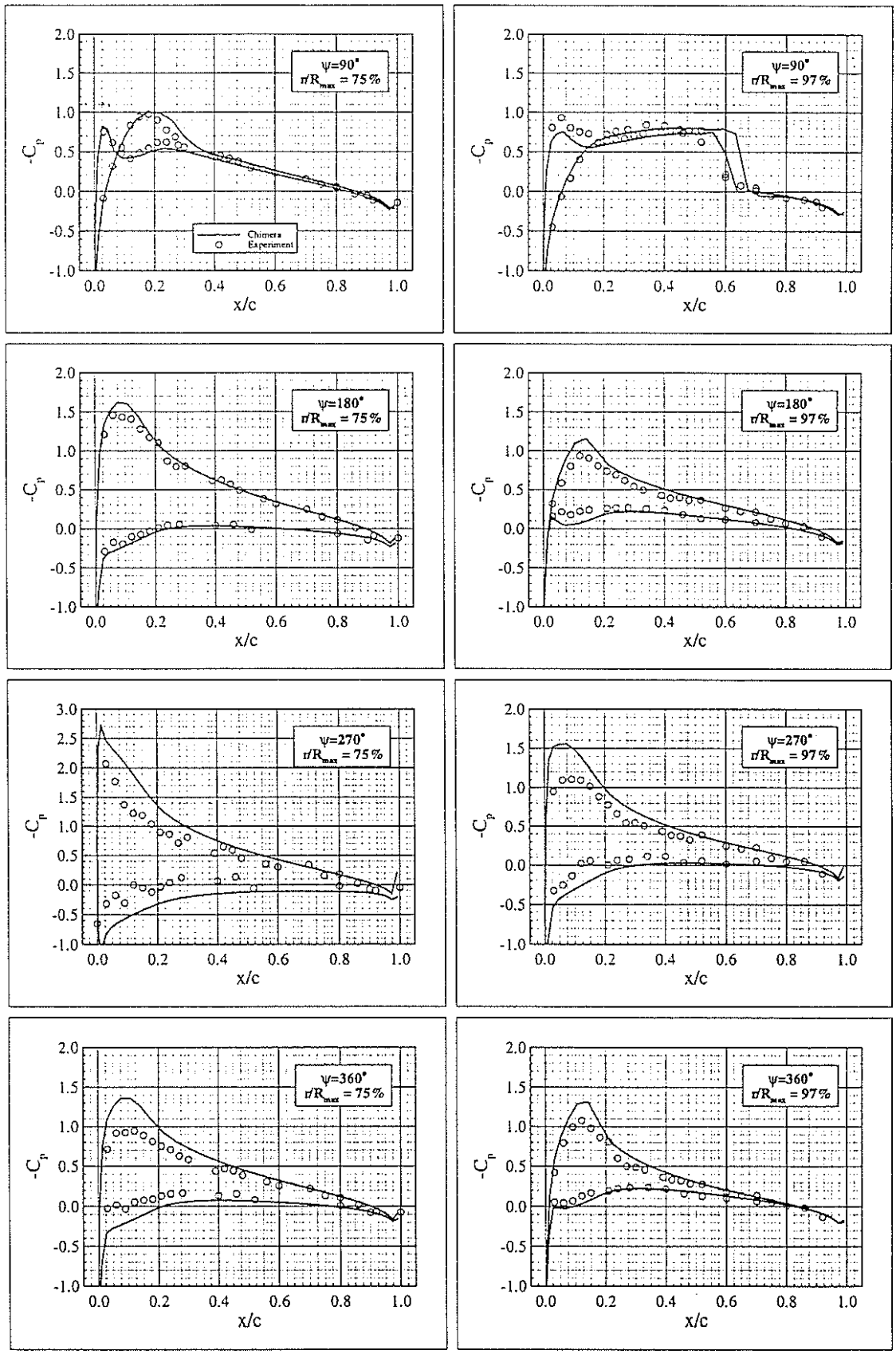

Figure 19: Chordwise Pressure Distributions DP–1839